Hindawi
Advances in Materials Science and Engineering
Volume 2022, Article ID 5375810, 11 pages
https://doi.org/10.1155/2022/5375810

*Research Article*

# Chloride Adsorption on EDTA Intercalated MnFe-LDHs: Characterization, Performance, and Application

**Xue Han**

*School of Architecture and Engineering, Chongqing Industry Polytechnic College, Chongqing 401120, China*

Correspondence should be addressed to Xue Han; hanxue@cqipc.edu.cn

Received 24 July 2022; Revised 2 November 2022; Accepted 4 November 2022; Published 9 December 2022

Academic Editor: Guoqiang Xie



Ethylenediamine tetraacetate-intercalated Fe-Mn layered double hydroxides (MnFe-EDTA-LDHs) were prepared by coprecipitation. The influence of different factors on $Cl^-$ adsorption by MnFe-EDTA-LDHs was investigated. Additionally, MnFe-EDTA-LDHs were incorporated into the concrete to study the $Cl^-$ erosion properties. The result showed that the $Cl^-$ adsorption on MnFe-EDTA-LDHs was affected by the initial pH, dosage, and coexisting anions. The $Cl^-$ adsorption process by MnFe-EDTA-LDHs accorded with the pseudo-second-order model and the Redlich–Peterson model. The maximum adsorption capacity of $Cl^-$ on MnFe-EDTA-LDHs reached 129.50 mg/g. The adsorption mechanism involved the complexation of O-containing groups, ion exchange, and electrostatic interaction. Moderate additions of MnFe-EDTA-LDHs improved the resistance of the concrete to $Cl^-$ erosion, while excessive additions reduced the $Cl^-$ erosion resistance. This work indicated that MnFe-EDTA-LDHs effectively retarded the $Cl^-$ erosion on concrete.

## 1. Introduction

Concretes are widely used in marine construction (e.g., terminals, ports, cross-sea bridges, and offshore exploration platforms). However, high concentrations of chloride ions reduce the durability of concrete structures [1, 2]. Additionally, the chlorides lead to concrete fragmentation and deterioration [3]. To reduce the permeability of chloride ions, it is necessary to delay the transport of chloride ions in concrete. Surface coatings and corrosion inhibitors are the common methods to prevent concrete corrosion [4, 5]. Organic coatings have poor-wear resistance and low-impact resistance, while inorganic coatings are less adherent and flexible. Corrosion inhibitors can reduce the concrete corrosion, but there are difficulties in dispersion [6, 7]. The development of methods for effective chloride adsorption in concrete is essential.

In recent years, the addition of layered double hydroxides ( LHDs ) to concrete can delay the transfer of $Cl^-$ [8]. The chemical formula for LDHs is as follows: $[M_{1-x}^{2+}M_x^{3+}(OH)_2]^{x+}[A_{x/n}^{n-}\bullet H_2O]^{x-}$, where $M^{2+}$ and $M^{3+}$ are divalent and trivalent metal cations [9–11]. Therefore, LDHs become a promising material for adsorbing chloride ions [8]. LDHs with inserted inhibitory anions can act as chloride ion adsorbents. On the one hand, LDHs can reduce the number of chloride ions in the aqueous solution [4, 12]. On the other hand, LDHs can release the inhibitory anions to prevent the $Cl^-$ into the concrete structure [13, 14]. Wang et al. [15] showed that MgAl-$NO_2$-LDH effectively inhibited the $Cl^-$ and $SO_4^{2-}$ in cement mortar. The presence of $SO_4^{2-}$ affected the amount of $Cl^-$ uptake, and there was a coupling effect of $Cl^-$ and $SO_4^{2-}$ on their penetration into the mortar specimens. Xu et al. [16] found that the $Cl^-$ adsorption of CaMnFe-LDHs with $NO^-_3$ intercalation was chemisorption, and the $NO^-_3$ exchanged with $Cl^-$. Additionally, Yang et al. [14] reported that the MgAl-LDHs prepared by the supergravity rotating bed method had a more regular and homogeneous structure. The adsorption capacity of $Cl^-$ was 3 times higher after calcination of the MgAl-LDHs. The insertion of inhibitory anions into LDHs can enhance the adsorption of $Cl^-$. The inhibitory anions released into the aqueous solution can prevent the $Cl^-$ into the concrete structure. Wei et al. [4] prepared aminobenzoate-intercalated MgAl-LDHs to adsorb $Cl^-$ from aqueous solutions, and

the adsorption process was spontaneous and exothermic. The corrosion inhibition of concrete was due to the $Cl^-$ adsorption by 2-mercaptobenzothiazole-intercalated ZnAl-LDHs [17]. Inhibitory anionic intercalation of LDHs provides good inhibition of concrete against $Cl^-$ corrosion. As mentioned above, the $Cl^-$ adsorption performance of LDHs is a key factor in the ability to inhibit $Cl^-$ corrosion. The adsorption performance of LDHs with EDTA intercalation on $Cl^-$ has rarely been reported.

In this work, EDTA intercalated MnFe-LDHs (MnFe-EDTA-LDHs) were prepared. Different influencing factors on the $Cl^-$ removal by MnFe-EDTA-LDHs were investigated. Meanwhile, the resistance of LDHs to $Cl^-$ erosion on the concrete was explored. This work provided a theoretical basis for the resistance of concrete to $Cl^-$ erosion.

## 2. Materials and Methods

*2.1. Reagents.* $Mn(NO_3)_2{\cdot}4H_2O$, $Fe(NO_3)_3{\cdot}9H_2O$, EDTA-Na, and NaCl were analytical reagents. All reagents were purchased from Sinopharm Reagent Group (Shanghai, China). The water used in the experiments was deionized water (DW). The cement was conventional P·O 42.5 cement with a density of 3.06 g/cm$^3$. The main substances of cement were $SiO_2$ (27.68%), CaO (49.73%), $Al_2O_3$ (10.09%), $Fe_2O_3$ (3.18%), MgO (1.97%), and others (7.35%).

*2.2. Preparation of Materials.* Preparation of FeMn-EDTA-LDHs: 4.569 g $Mn(NO_3)_2{\cdot}4H_2O$ and 3.617 g $Fe(NO_3)_3{\cdot}9H_2O$ were dissolved in 50 mL DW to obtain Fe-Mn hybrid solution. 9.6 g NaOH and 4.653 g EDTA-Na were dissolved in 100 mL DW, and the solution was stirred to get the alkali mixed solution. Then, two mixtures were mixed in a triple flask, and the solution pH was adjusted to 12.0 by 0.1 mol NaOH. The flask was continuously filled with $N_2$ and transferred to a water bath at 60°C for 6 h. The reaction product was cooled to room temperature and washed three times by DW. The product was dried in a vacuum freeze dryer for 24 h, which was FeMn-EDTA-LDHs.

*2.3. Adsorption Experiments.* All adsorption experiments were conducted with a 150 mL conical flask oscillated in a shaker of 150 r/min at 25°C. The pH was adjusted by infinitesimal NaOH or $HNO_3$ solution at 0.1 mol/L. The effect of initial solution pH was investigated between 2.0 and 11.0 at 50 mg/L $Cl^-$. Different dosage (0.1~3 g/L) of FeMn-EDTA-LDHs was added to the $Cl^-$ solution to investigate the dosage effects. The mixed solutions of 50 mg/L $Cl^-$ and coexist ions ($Na^+$, $K^+$, $Ca^{2+}$, $Mg^{2+}$, $Fe^{3+}$, $SO_4^-$, $NO_3^-$, $CO_3^{2-}$, $PO_4^{3-}$, and $SiO_3^{2-}$) were configured. The concentration of coexisting ions was set to 0.001, 0.01, and 0.1 mol/L. The effect of coexisting ions for $Cl^-$ adsorption was investigated. The effect of different temperatures (15°C~50°C) on the $Cl^-$ removal by FeMn-EDTA-LDHs was investigated. For adsorption kinetics experiments, the reaction time was set to form 10 min~600 min. For isotherm experiments, the $Cl^-$ concentration was set from 50 to 1000 mg/L. All experiments were repeated three times. Additionally, adsorption-desorption experiments were carried out on FeMn-EDTA-LDHs using NaOH as a desorbent.

*2.4. Data Analysis.* After the reaction was completed, 10 mL solution was centrifuged for 10 min and the $Cl^-$ concentration of the solution was measured using a chloride ion content measuring instrument (NJCL-B, Meiyu, Shanghai, China). The removal efficiency (Equation (1)) and the adsorption capacity (Equation (2)) were calculated.

$$R = \frac{C_0 - C_e}{C_0} \times 100\%, \tag{1}$$

$$Q = \frac{(C_0 - C_e) \times V}{m}, \tag{2}$$

where $R$ (%) is the removal efficiency; $C_0$ (mg/L) and $C_e$ (mg/L) are the initial concentration of $Cl^-$ and the remaining concentration of $Cl^-$ in the solution after adsorption equilibrium, respectively; $q_e$ (mg/g) is the $Cl^-$ adsorption capacity of FeMn-EDTA-LDHs, mg/g; $V$ (mL) is the volume of the solution; and $m$ (mg) is the dosage of the FeMn-EDTA-LDHs.

The effect of adsorption time (10~600 min) on the $Cl^-$ removal was investigated at 25°C, dosage 1 g/L, $Cl^-$ concentration 50 mg/L, and pH 7.0. The experimental data were fitted and analysed using the pseudo-first-order model (3), the pseudo-second-order model (4), the Elovich model (5), the intraparticle diffusion model (6),and the Boyd kinetic model (7).

$$q_t = q_e\left(1 - e^{-k_1 t}\right), \tag{3}$$

$$q_t = \frac{q_e^2 k_2 t}{1 + q_e k_2 t}, \tag{4}$$

$$q_t = \frac{1}{\beta}\ln\left(1 + \alpha\beta t\right), \tag{5}$$

$$q_t = K_d t^{1/2} + C_i, \tag{6}$$

$$B_t = -0.4977 - \ln\left(1 - F\right) F = \frac{q_t}{q_\alpha}, \tag{7}$$

where $q_e$ and $q_t$ are the adsorption capacity at adsorption equilibrium and at a time "$t$," respectively, mg/g; $k_1$ (min$^{-1}$) and $k_2$ (g/mg·min) are adsorption rate constant of the pseudo-first-order and the pseudo-second-order model, respectively; $\alpha$ (mg/g·min) and $\beta$ are the initial absorbance and desorption constant, respectively; $K_d$ (mg/m·min$^{1/2}$) is the intraparticle diffusion constant; $C_i$ is the boundary layer constant; $q_\alpha$ represents the amount sorbed (mg/g) at the infinite time; and $B_t$ is a mathematical function of $F$. The $B_t$ values at different contact times were calculated. The calculated $B_t$ values were plotted against time $t$ (min).

The effect of the initial concentration (50~1000 mg/L) on the $Cl^-$ removal was investigated at pH 7.0, a dosage of 1 g/L, and 600 min. The experimental data were fitted and analysed by Langmuir (8), Freundlich (9), Temkin (10), Sips (11),

Redlich–Peterson (12), Toth (13),and Hill (14)isotherm models.

$$q_e = \frac{q_{\max} K_L C_e}{1 + K_L C_e}, \tag{8}$$

$$q_e = K_f C_e^{1/n}, \tag{9}$$

$$q_e = \frac{RT}{b_T} \ln (A_T C_e), \tag{10}$$

$$q_e = \frac{K_s C_e^{\beta_H}}{1 + a_s C_e^{\beta_H}}, \tag{11}$$

$$q_e = \frac{K_R C_e}{1 + a_R C_e^{\beta}}, \tag{12}$$

$$q_e = \frac{K_T C_e}{(a_T + K_T C_e)^{1/n}}, \tag{13}$$

$$q_e = \frac{Q_{s_H} C_e^{n_H}}{K_D + C_e^{n_H}}, \tag{14}$$

where $q_e$ (mg/g) is the adsorption capacity at equilibrium, mg/g; $C_e$ (mg/L) is the $Cl^-$ concentration at adsorption equilibrium; $q_{\max}$ (mg/g) and $K_L$ (L/mg) are the theoretical maximum adsorption capacity and the Langmuir equilibrium constant, respectively; $K_f$ ($mg^{1-n} \cdot L^n/g$) and $n$ are the Freundlich equilibrium constant and dimensionless number, respectively; $A_T$ (1/g) and $b_T$ (kJ/mol) are Temkin constants; $R$ is the global constant of gases (8.314 $kJ \cdot mol^{-1}$), and $T$ is the absolute temperature (K). $K_s$ (mg/g), $K_T$ (mg/g), and $Q_{SH}$ (mg/g) are the maximum adsorption capacity. $A_s$ (L/mg) and $\beta_s$ are the Sips isotherm constants. $K_R$ (L/g), $a_R$ (L/mg), and $\beta$ are the Redlich–Peterson isotherm constants. $a_T$ (L/mg) is the Toth isotherm constant. $K_D$ is the Hill constant. $n_H$ is the cooperativity coefficient of binding interaction obtained from the slope of a Hill plot.

*2.5. Immobilisation Experiments.* The concrete samples (size: 60 mm × 60 mm × 60 mm) were prepared by mixing a certain amount of FeMn-EDTA-LDHs as an admixture. The concrete specimens are prepared as shown in Table 1. The concrete samples were placed in 5% chloride solution after 28 d curing. The concrete samples were immersed at room temperature for 30 and 60 d.

After soaking, the concrete samples were dried in a drying oven at 60°C for 24 h. The concrete samples were cut into small pieces at 2 mm intervals and broken into powder. Subsequently, the powder was mixed with 100 mL of DW and soaked for 24 h. The mixture was filtered, and the filtrate was collected. Finally, the $Cl^-$ concentration in the filtrate was measured using a chloride ion content meter. The mass fraction of $Cl^-$ at different depths of the concrete samples was calculated.

*2.6. Structural Characterisation of the Materials.* The surface morphology structure was analysed by the scanning electron microscope (SEM, JSM-7500F, Electronics, Japan). Surface elemental analysis is done by energy dispersive spectroscopy (EDS, JSM-2100F, Electronics, Japan). Zeta potential analyser (ZS-90, Malvern, UK) analyses the surface potential of FeMn-Cl-LDHs at different pH and calculates zero potential point. The crystalline structure was analysed by an X-ray Diffraction (XRD, D8, Bruker, Germany). The functional groups of FeMn-EDTA-LDHs before and after adsorption were investigated by Fourier transform interferometric radiometer (FTIR, Nicolet460, Thermo Fisher Scientific, USA).

## 3. Results and Discussion

*3.1. Characterization Analysis.* Figure 1 shows that FeMn-EDTA-LDHs morphological features are observed by SEM. Before the reaction (Figure 1(a)), the surface was rough and loose, showing an irregular lamellar structure with sharp angles [18]. After $Cl^-$ adsorption (Figure 1(b)), the structure of FeMn-EDTA-LDHs was stacked, agglomerated, and collapsed. By EDS analysis, the elements of C (31.89%), O (26.10%), Mn (27.68%), and Fe (14.33%) were present in the FeMn-EDTA-LDHs before adsorption. Additionally, the ratio of Mn to Fe was exactly 2 : 1, which was consistent with the ratio used in the preparation. After adsorption (Figure 1(b)), the element of chlorine appeared in the EDS, which indicated that the FeMn-EDTA-LDHs adsorbed $Cl^-$ from the aqueous solution.

The $N_2$ adsorption-desorption isotherm of FeMn-EDTA-LDHs is displayed in Figure 2(a). The adsorption-desorption isotherms were classified as type IV isotherms [19, 20]. The pore size distribution (Figure 2(b)) of FeMn-EDTA-LDHs was 2~50 nm, which demonstrated that FeMn-EDTA-LDHs were mesoporous materials [7]. The specific surface area and pore size of FeMn-EDTA-LDHs were 115.38 $m^2/g$ and 17.24 nm, respectively.

The function group of FeMn-EDTA-LDHs before and after adsorption is shown in Figure 2(c). The strong and broad diffraction peak at 3420 $cm^{-1}$ was identified as the –OH [14, 21]. FeMn-EDTA-LDHs held an absorption band near 1600 $cm^{-1}$, which was a superposition of C=C/C=O functional groups in the carboxyl group [4, 21]. The band at 1411 $cm^{-1}$ corresponded to the asymmetric vibration peak of –COOH, which indicated the successful intercalation of EDTA. After the reaction, the –OH diffraction peak remained at 3435 $cm^{-1}$. However, the intensity and wavenumber of the –OH peaks were weakened and shifted, respectively. This phenomenon may attribute to a complex between the –OH and $Cl^-$ [3, 20]. Furthermore, the characteristic peak at 545 $cm^{-1}$ was the Mn-O and Fe-O functional groups [1, 16]. After adsorption, the Fe-O and Mn-O peaks shifted lower wavenumbers, which attributed to the complexation of Fe-O and Mn-O groups with $Cl^-$ [13].

The XRD analysis of the FeMn-EDTA-LDHs is shown in Figure 2(d). At $2\theta$ of 11.54°, 23.32°, 33.03°, 57.16°, and 58.66° were typical diffraction peaks of layered double hydroxides

Table 1: Proportioning of cement slurries.

| | Cement (g) | DW (mL) | FeMn-EDTA-LDHs (%) |
|---|---|---|---|
| C0 | 400 | 160 | 0 |
| C1 | 400 | 160 | 1 |
| C2 | 400 | 160 | 2 |
| C3 | 400 | 160 | 3 |
| C4 | 400 | 160 | 4 |

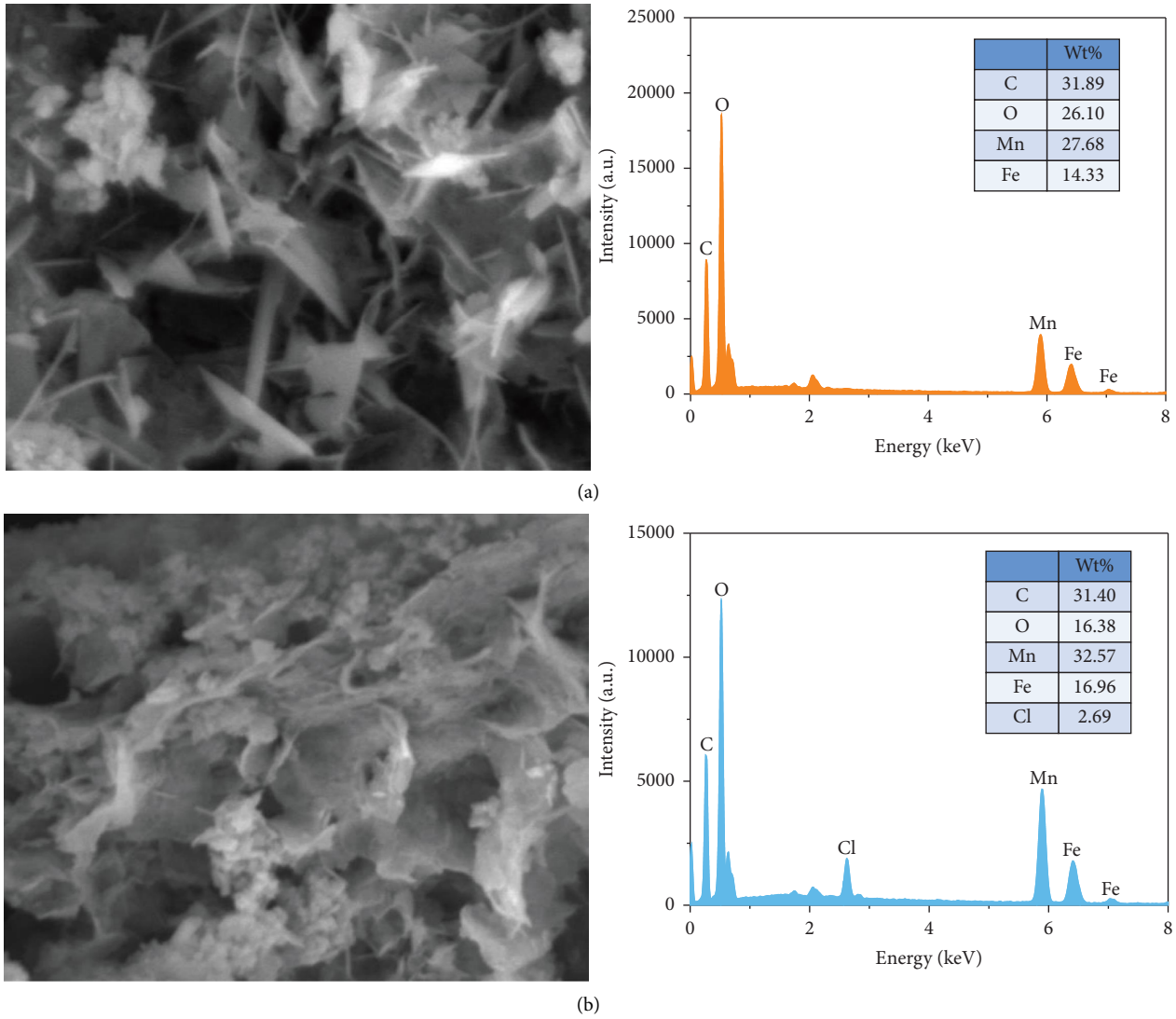


Figure 1: SEM-EDS images of $Cl^-$ before (a) and after (b) adsorption by FeMn-EDTA-LDHs.

[7, 16, 22]. This peak was corresponded to the (003), (006), (009), (110), and (113) diffraction crystallographic planes, respectively [16]. The intensity of the peaks after adsorption was reduced. This may be due to the ion exchange caused by chloride ion adsorption, which changed the charge density [23]. This indicated that the $Cl^-$ entered the crystals' interior during the adsorption process, causing changes in the lattice structure [9, 23]. The weakening of characteristic peaks was due to the collapse and plugging of the material structure after adsorption, which was consistent with the SEM result [4].

*3.2. Dosage.* The effect of the dosage on $Cl^-$ adsorption is shown in Figure 3(a). The unit adsorption capacity decreased rapidly when the dosage was increased from 0.1 g/L to 1 g/L. The dosage exceeded 1 g/L, and the unit adsorption capacity decreased slightly. With increasing dosage, the active site increased, andthe removal efficiency rose [24]. The removal efficiency increased very little when the dosage exceeded 1 g/L. This was considered to be the limited availability of $Cl^-$ in solution. Therefore, 1 g/L was supposed to be the optimum dosage for this work.

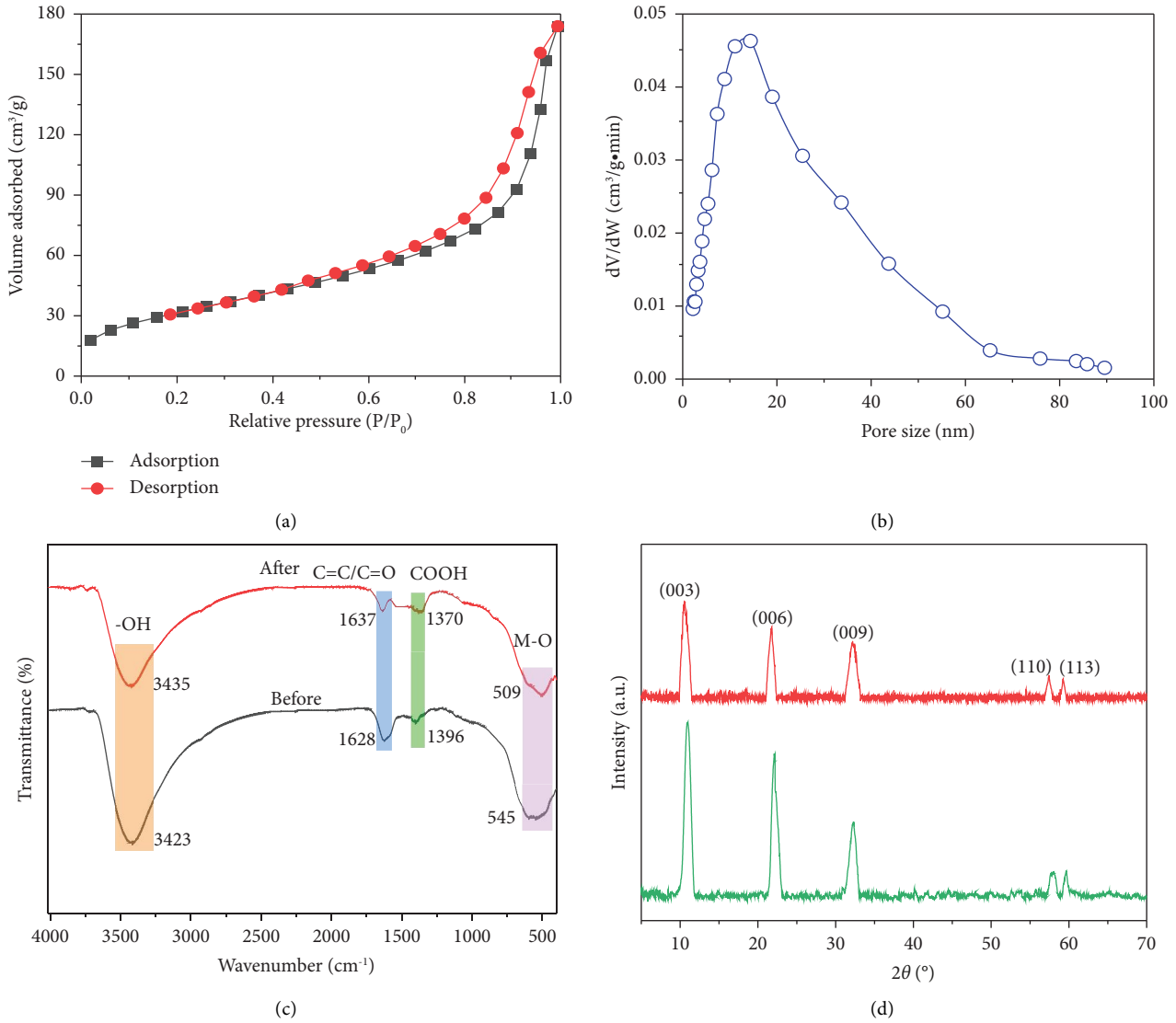


Figure 2: $N_2$ adsorption-desorption curves (a), pore size distribution (b), FTIR (c), and XRD (d) of MnFe-EDTA-LDHs.

*3.3. Initial Solution pH.* The effect of the initial solution pH on the $Cl^-$ adsorption by FeMn-EDTA-LDHs is shown in Figure 3(b). The $Cl^-$ adsorption capacity increased in the pH of 2.0~7.0. At pH > 7, the adsorption capacity dropped sharply to 11.55 mg/g. The zero potential point (pHpzc) of FeMn-EDTA-LDHs was 7.42 (Figure 3(c)). The solution pH was below 7.42, and the $H^+$ occupied the O-containing groups on the FeMn-EDTA-LDHs surface. The O-containing groups on the FeMn-EDTA-LDHs surface protonated and carried positive electricity, and the $Cl^-$ adsorption capacity was enhanced. When the solution pH was higher than 7.42, the O-containing groups deprotonated, and the $Cl^-$ adsorption capacity was weakened [4, 7, 18]. Thus, the electrostatic interaction between $Cl^-$ and FeMn-EDTA-LDHs played a role in the removal process.

*3.4. Coexisting Ions.* The effect of coexisting cations on $Cl^-$ adsorption was investigated (Figure 3(d)). However, the adsorption efficiency was barely affected by increasing the concentration of $Na^+$, $K^+$, $Ca^{2+}$, $Mg^{2+}$, and $Fe^{3+}$ from 0 to 0.1 mol/L. This indicated that the cations had almost no effect on the $Cl^-$ removal from aqueous solutions by FeMn-EDTA-LDHs. The effect of coexisting anions on $Cl^-$ adsorption was researched (Figure 3(e)). Nitrate had no perceptible impact on the $Cl^-$ removal. Sulphate, carbonate, silicate, and phosphate had an obvious inhibitory effect on the $Cl^-$ removal [16]. The order of impact was carbonate > sulphate > silicate > phosphate.

*3.5. Adsorption Temperature.* This work examined the effect of adsorption temperature (15°C~50°C), and the results are shown in Figure 3(f). The removal efficiency decreased with increasing temperature. This result indicated that the adsorption process was exothermic and that high temperature reduced the removal efficiency. Previous literature showed that high temperatures decreased the $Cl^-$ adsorption efficiency [4].

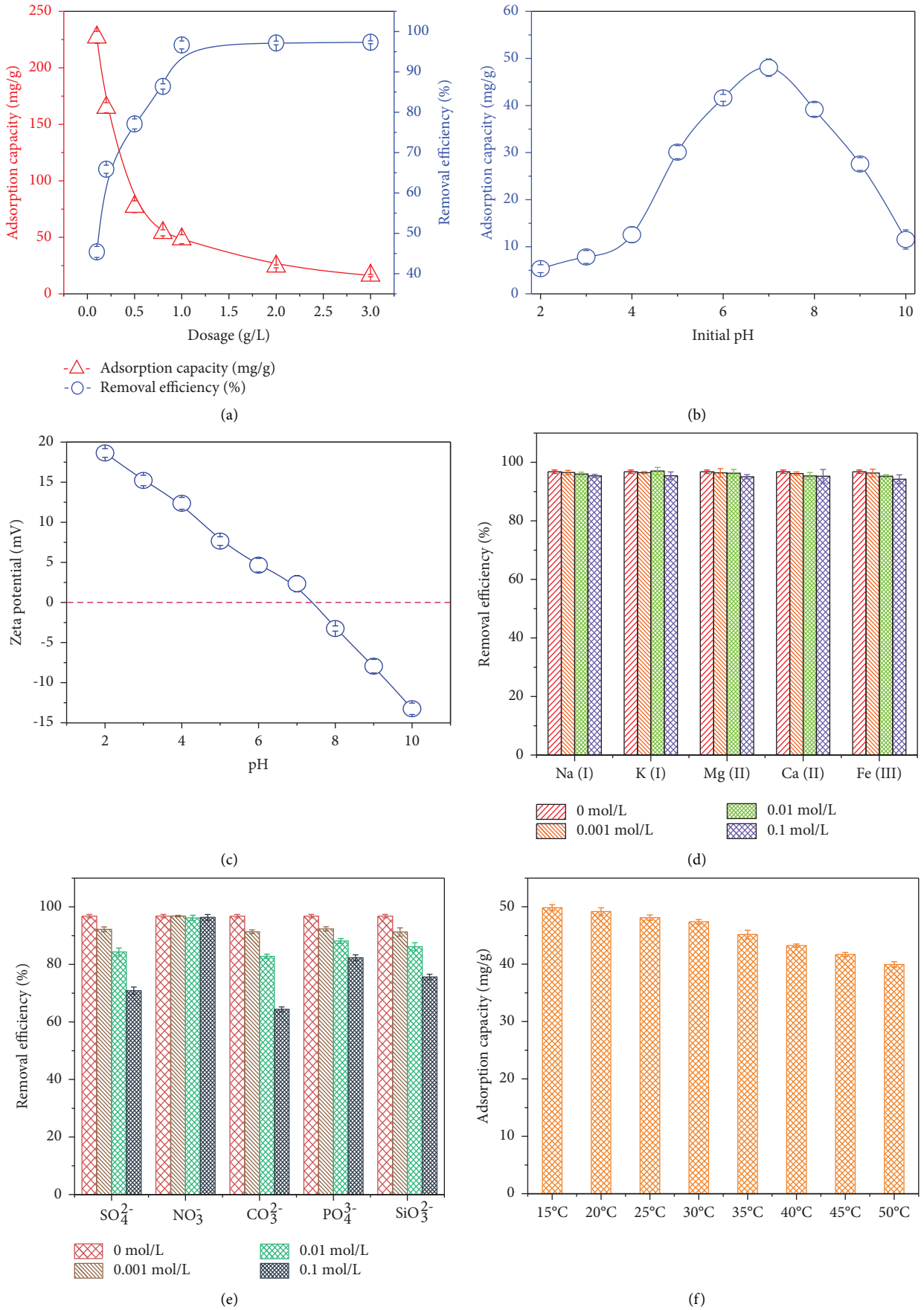


Figure 3: The effects of dosage (a) and initial solution pH (b) on the $Cl^-$ removal by FeMn-EDTA-LDHs. Zeta potential of FeMn-EDTA-LDHs at different pH (c). The effects of coexisting cations (d), coexisting anions (e), and adsorption temperature (f) on the $Cl^-$ removal by FeMn-EDTA-LDHs.

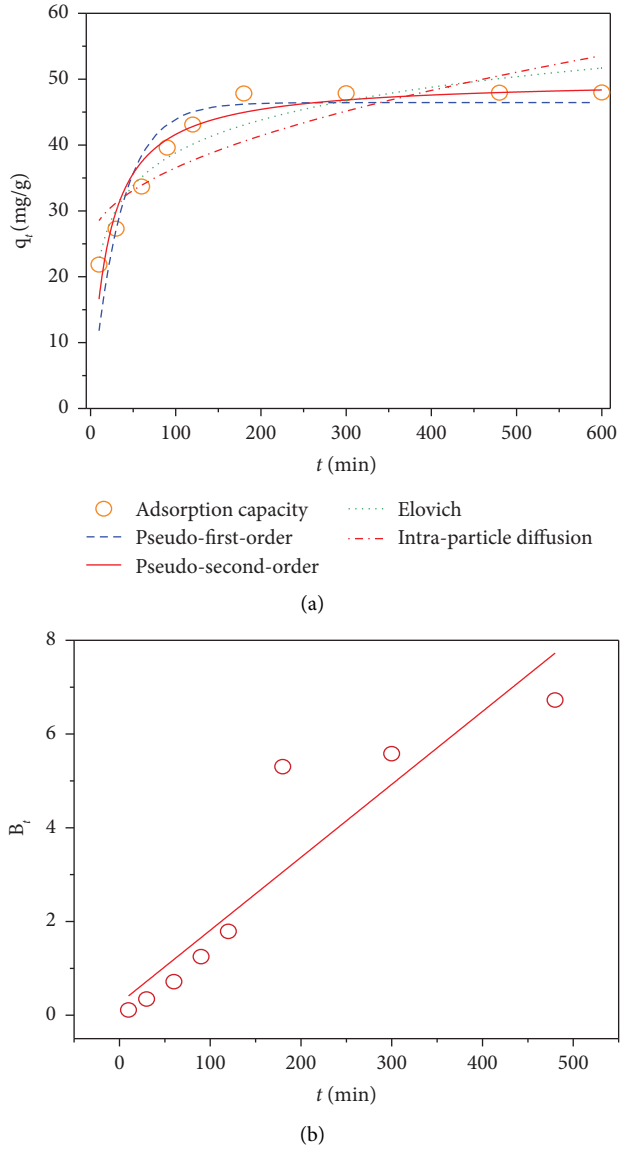


Figure 4: Adsorption kinetics model, (a) and Boyd kinetic model, (b) of Cl- removal by FeMn-EDTA-LDHs.

*3.6. Adsorption Kinetics.* Figure 4(a) shows that the $Cl^-$ adsorption capacity by FeMn-EDTA-LDHs increased rapidly from 21.85 mg/g to 33.69 mg/g within 10~30 min. Then, the $Cl^-$ adsorption capacity increased slowly to 47.97 mg/g within 30~600 min. The increase in adsorption between 10 and 30 min was attributed to the presence of abundant unused adsorption sites for FeMn-EDTA-LDHs [4, 5, 22].

Table 2 shows that the correlation coefficient ($R^2$) of the pseudo-second-order kinetic model ($R^2 = 0.923$) was higher than those of the pseudo-first-order kinetic model ($R^2 = 0.784$) and the Elovich model ($R^2 = 0.903$), indicating that the pseudo-second-order model can more accurately describe the $Cl^-$ adsorption process. This result suggested that the $Cl^-$ adsorption process was a chemical reaction (e.g., ion exchange or complexation) [3]. Previous studies demonstrated that O-containing groups on LDHs were capable of complexing with $Cl^-$ [16]. The data were analysed using an intraparticle diffusion model (Figure 4(a)). The fitted curve did not pass through the origin, suggesting that the adsorption process was influenced by various factors [16]. Therefore, the adsorption rate was affected by membrane diffusion and intraparticle diffusion. [14]. Additionally, the adsorption rate was influenced by the dosage, boundary layer resistance, and electrostatic interaction. Xu et al. [16] considered that membrane diffusion played a dominant role in the $Cl^-$ adsorption by LDHs. This was also consistent with the results of the present study. The Boyd model (Figure 4(b)) indicated that boundary layer/film diffusion predominantly determines the $Cl^-$ adsorption process.

*3.7. Adsorption Isotherms.* Figure 5 shows that the $Cl^-$ adsorption by FeMn-EDTA-LDHs first increased and reached stability. This was that LDHs had adequate active sites capable of reacting with chloride ions at low

Table 2: The kinetic model fitting parameters.

| Pseudo-first-order model | | | Pseudo-second-order model | | | Elovich model | | | Intraparticle diffusion model | | | Boyd kinetic model | | |
|---|---|---|---|---|---|---|---|---|---|---|---|---|---|---|
| $q_e$ | $k_1$ | $R^2$ | $q_e$ | $k_2$ | $R^2$ | $\alpha$ | $\beta$ | $R^2$ | $k_1$ | $C_1$ | $R^2$ | $k_2$ | $C_2$ | $R^2$ |
| 46.44 | 0.029 | 0.784 | 49.98 | 0.001 | 0.923 | 16.092 | 0.139 | 0.903 | 1.174 | 24.81 | 0.745 | 0.016 | 0.26 | 0.857 |

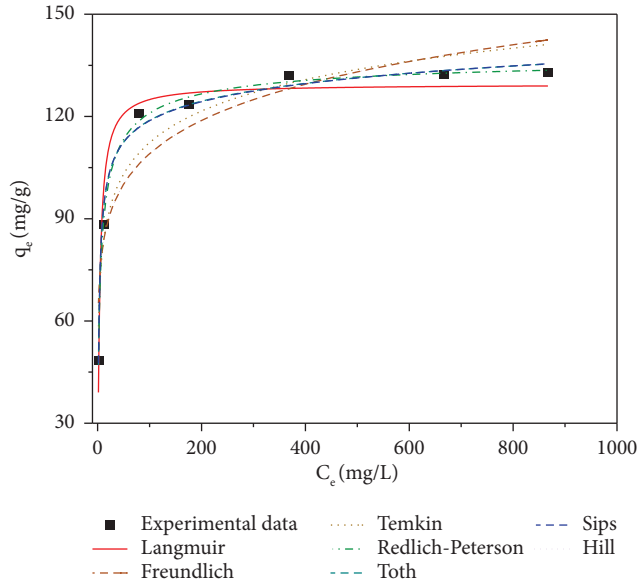


Figure 5: The adsorption-desorption experiments of FeMn-EDTA-LDHs.

concentrations. At high concentration, the active site on FeMn-EDTA-LDHs could not remove all the $Cl^-$ from the aqueous solution.

Table 3 shows that the correlation coefficients ($R^2$) for Freundlich and Hill were less than 0.8, indicating that these two models could not accurately account $Cl^-$ adsorption process. The $R^2$ of the other models were all above 0.9. The parameter of $q_{max}$ (129.50 mg/g), $K_s$ (55.77 mg/g), and $K_T$ (94.27 mg/g) indicated the maximum adsorption capacity. Then, $K_s$ and $K_T$ differed from the actual adsorption capacity (132.90 mg/g). So, neither the Sips nor the Toth model could better describe the $Cl^-$ adsorption process. The Langmuir model indicated that the $Cl^-$ adsorption process was monolayer adsorption [16, 24]. The $K_L$ value from 0 to 1 indicated that the adsorption process was favourable [24]. Based on the $K_L$ values, the adsorption of FeMn-EDTA-LDHs was favourable for $Cl^-$ [7, 18]. The maximum adsorption capacity was 129.50 mg/g. Notably, the maximum adsorption capacity (129.50 mg/g) was very close to the actual adsorption capacity (132.90 mg/g), which also indicated that the Langmuir model could better account for the removal process. Additionally, the Temkin model ($R^2 > 0.932$) described the experimental results well (Table 3). This result indicated that strong intermolecular forces existed between the $Cl^-$ and absorbent [16]. The Redlich–Peterson model indicated that the adsorption process was monolayer and multilayer adsorption [14, 16]. This suggested that the $Cl^-$ adsorption process was subject to multiple mechanisms (e.g., electrostatic interaction and complexation) [5]. Additionally, the $Cl^-$ adsorption capacity of different adsorbents was compared (Table 4). The $Cl^-$ adsorption capacity of FeMn-EDTA-LDHs was much higher than that of other adsorbents. This indicated that FeMn-EDTA-LDHs had an excellent $Cl^-$ adsorption capacity.

*3.8. Adsorption-Desorption Experiments.* In this experiment, 0.1 mol/L NaOH solution was used as the desorption solution and regenerated by shaking in a shaker at 30°C for 4 h at 150 rpm. The adsorption-desorption experiments were carried out 5 times (Figure 6). The $Cl^-$ removal efficiency by FeMn-EDTA-LDHs decreased slightly with an increasing number of cycles. The $Cl^-$ removal efficiency still maintained at over 90% after 5 regeneration cycles. The removal efficiency decreased was due to the reduction of functional groups and the blockage of the pore. This indicated that FeMn-EDTA-LDHs had excellent reproducible utility for $Cl^-$.

*3.9. Effect of FeMn-EDTA-LDHs on the $Cl^-$ Erosion Resistance of Concrete.* The $Cl^-$ concentration curve at different depths after the concrete was immersed in 5% NaCl solution is shown in Figure 7. The $Cl^-$ content in the concrete gradually decreased with depth. Notably, the experimental group C0 had a higher $Cl^-$ content than others. This result indicated that FeMn-EDTA-LDHs could enhance the ability of the concrete to resist $Cl^-$

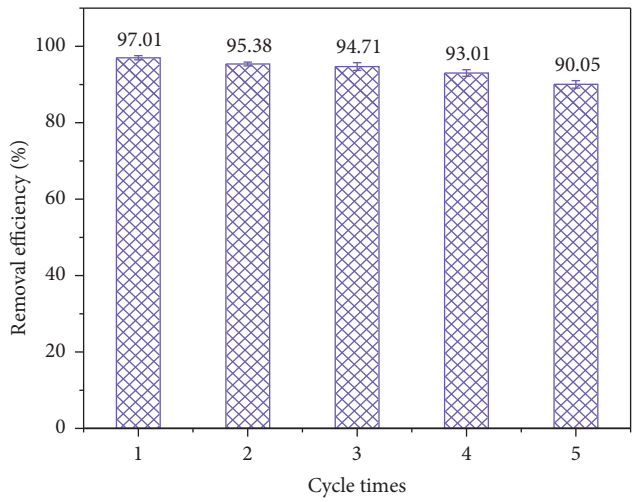


Figure 6: Isothermal adsorption model.

Table 3: Fitting parameters of the adsorption isotherm.

| Model | Parameter | |
|---|---|---|
| Langmuir | Actual adsorption capacity | 132.90 |
| | $q_{max}$ | 129.50 |
| | $K_L$ | 0.276 |
| | $R^2$ | 0.958 |
| Freundlich | $K_f$ | 61.74 |
| | $n$ | 8.090 |
| | $R^2$ | 0.860 |
| Temkin | $b_T$ | 46.33 |
| | $A_T$ | 13.31 |
| | $R^2$ | 0.932 |
| Sips | $Ks$ | 55.756 |
| | $\beta_s$ | 0.615 |
| | $a_s$ | 0.402 |
| | $R^2$ | 0.997 |
| Redlich–Peterson | $K_R$ | 56.243 |
| | $a_R$ | 0.587 |
| | $\beta$ | 0.948 |
| | $R^2$ | 0.986 |
| Toth | $K_T$ | 94.274 |
| | $a_T$ | 1.842 |
| | $n$ | 1.057 |
| | $R^2$ | 0.989 |
| Hill | $Q_{sH}$ | 259.53 |
| | $n_H$ | 0.124 |
| | $K_D$ | 4.272 |
| | $R^2$ | 0.825 |

erosion. Furthermore, the proportion of FeMn-EDTA-LDHs increased, and the $Cl^-$ content increased then decreased. The $Cl^-$ content in the concrete was lowest when the incorporation amount of FeMn-EDTA-LDHs was 3%. In addition, the $Cl^-$content of the C4 group was higher than that of the C3 group. This phenomenon was contributed to the expansion of concrete pore structure by the excess LDHs, which weakened the resistance of concrete to $Cl^-$ infiltration [16]. Previous studies were also consistent with the results of this work [15, 16].

With the increase of erosion time, the concentration of $Cl^-$in concrete is higher. This suggested that the water-soluble $Cl^-$ gradually diffused into the concrete. The $Cl^-$ content in the concrete at 60 d was higher than that at 30 d. Therefore, the $Cl^-$ continued to erode and transport into the concrete, and the erosion deepened over time until the

Table 4: Comparison of the $Cl^-$ adsorption capacity of different adsorbents.

| Adsorbent | $Q_{max}$ (mg/g) | References |
|---|---|---|
| CaAl-Cl-LDH | Approximately 25 mg/g | [5] |
| MgAl-LDHs intercalated with aminobenzoate ions | 32.16 mg/g | [4] |
| CNTs/MgAl-LDHs | 75.58 mg/g | [3] |
| MgAl-LDHs | 34.82 mg/g | [14] |
| CaMnFe-LDHs | 144.01 mg/g | [16] |
| MnFe-EDTA-LDHs | 129.50 mg/g | This work |

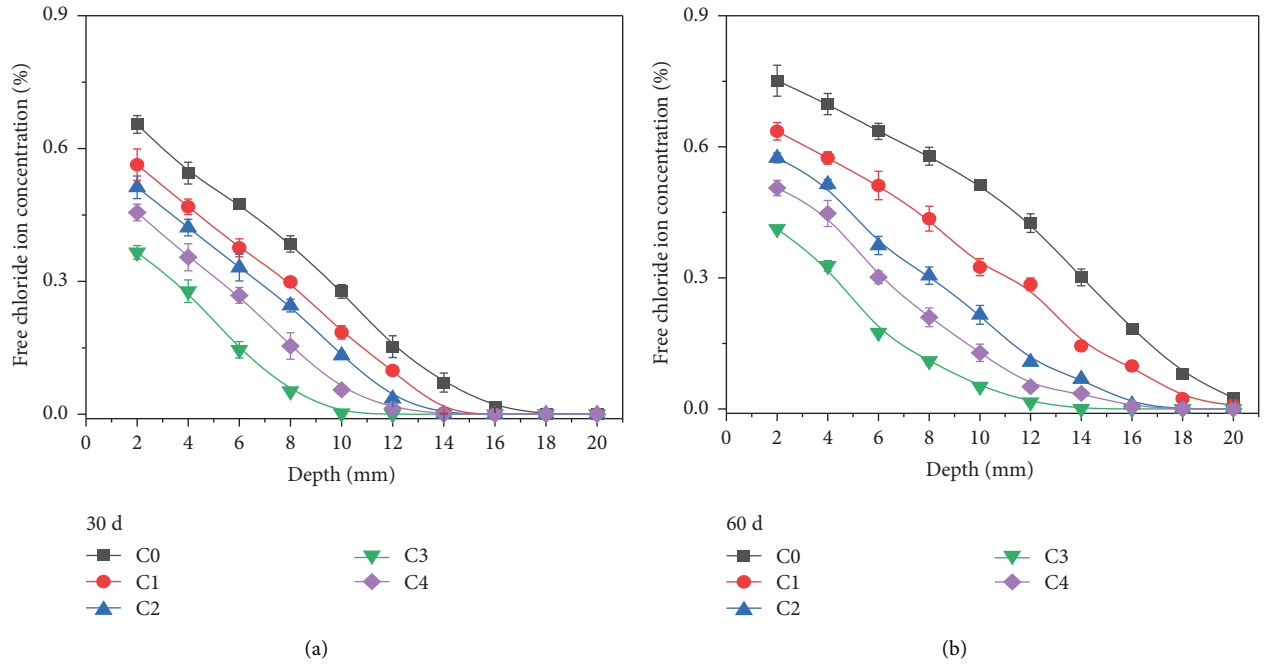


Figure 7: The distribution of $Cl^-$ concentration in concrete at 30 d (a) and 60 d (b).

equilibrium dynamic [1, 6, 25]. This work showed that moderate of FeMn-EDTA-LDHs could effectively enhance the resistance of concrete to $Cl^-$ erosion.

## 4. Conclusions

FeMn-EDTA-LDHs were prepared by coprecipitation. The pseudo-second-order and the Redlich–Peterson models provided a better fit for the experimental data. The $Cl^-$ adsorption capacity on MnFe-EDTA-LDHs reached 129.50 mg/g. At dosage 1 g/L and initial pH 7.0, FeMn-EDTA-LDHs held better $Cl^-$ removal efficiency. The cations barely affected the $Cl^-$ removal from aqueous solutions by FeMn-EDTA-LDHs. Sulphate, carbonate, silicate, and phosphate obviously inhibited the $Cl^-$ removal. The removal mechanism is involved in the complexation of O-containing groups, ion exchange, and electrostatic interaction. Moderate of MnFe-EDTA-LDHs improved the resistance of concrete to $Cl^-$ erosion, while excessive additions led to a reduction in the $Cl^-$ erosion resistance. This work indicated that FeMn-EDTA-LDHs retarded the $Cl^-$ erosion on concrete. The mechanism by which LDHs improved the resistance of cement samples to $Cl^-$ erosion will be explained by more means in next works.

## Data Availability

The data used to support the findings of this study are included within the article.

## Conflicts of Interest

The author declares that there are no conflicts of interest.

## Acknowledgments

This work was supported by the Science and Technology Research Program of Chongqing Municipal Education Commission (Grant No. KJQN202003204).

## References

[1] Y. X. Chen, Z. H. Shui, and W. Chen, "Chloride binding of synthetic Ca-Al-$NO_3$ LDHs in hardened cement paste," *Construction and Building Materials*, vol. 93, pp. 1051–1058, 2015.

[2] X. Ke, S. A. Bernal, and J. L. Provis, "Uptake of chloride and carbonate by Mg-Al and Ca-Al layered double hydroxides in simulated pore solutions of alkali-activated slag cement," *Cement and Concrete Research*, vol. 100, pp. 1–13, 2017.

[3] G. J. Ke, Z. Zhou, P. F. Yang, and B. X. Song, "Preparation of CNTs/MgAl-LDHs composites and their adsorption properties for chloride ions," *Materials Science Forum*, vol. 956, pp. 305–313, 2019.

[4] J. F. Wei, J. X. Xu, Y. J. Mei, and Q. Tan, "Chloride adsorption on aminobenzoate intercalated layered double hydroxides: kinetic, thermodynamic and equilibrium studies," *Applied Clay Science*, vol. 187, Article ID 105495, 2020.

[5] L. Chi, Z. Wang, Y. Zhou, S. Lu, and Y. Yao, "Layered double hydroxides precursor as chloride inhibitor: synthesis, characterization, assessment of chloride adsorption performance," *Materials*, vol. 11, no. 12, p. 2537, 2018.

[6] Y. H. Cao, S. G. Dong, D. J. Zheng et al., "Multifunctional inhibition based on layered double hydroxides to comprehensively control corrosion of carbon steel in concrete," *Corrosion Science*, vol. 126, pp. 166–179, 2017.

[7] S. P. Zhang, F. Yu, W. T. He et al., "Experimental investigation of chloride uptake performances of hydrocalumite-like Ca-Al LDHs with different microstructures," *Applied Sciences*, vol. 10, no. 11, pp. 3760–3775, 2020.

[8] H. H. Chen, L. R. Yuan, and M. X. Li, "Research progress in Technology of chloride removal from aqueous solution," *Journal of Materials Protection*, vol. 48, pp. 31–35, 2015.

[9] Y. R. Hu, H. B. Li, Q. Wang, J. Zhang, and Q. Song, "Characterization of LDHs prepared with different activity MgO and resisting $Cl^-$ attack of concrete in salt lake brine," *Construction and Building Materials*, vol. 229, Article ID 116921, 2019.

[10] T. Liu, Y. X. Chen, Q. L. Yu, J. Fan, and H. Brouwers, "Effect of MgO, Mg-Al-$NO_3$ LDH and calcined LDH-$CO_3$ on chloride resistance of alkali activated fly ash and slag blends," *Construction and Building Materials*, vol. 250, Article ID 118865, 2020.

[11] G. S. Li, J. P. Zhu, and G. Gao, "Research progress on influence of 2D nano materials on properties of cement-based materials," *Bulletin of the Chinese Ceramic Society*, vol. 37, pp. 3360–3364, 2018.

[12] B. Wu, J. D. Zuo, B. Q. Dong, F. Xing, and C. Luo, "Study on the affinity sequence between inhibitor ions and chloride ions in MgAl layer double hydroxides and their effects on corrosion protection for carbon steel," *Applied Clay Science*, vol. 180, Article ID 105181, 2019.

[13] J. X. Xu, Q. P. Tan, and L. H. Jiang, "Influence of $SO_4^{2-}$ on adsorption of $Cl^-$ and rust resistance of MgAl-LDHs," *Journal of Southeast University*, vol. 49, pp. 507–513, 2019.

[14] P. F. Yang, X. Yuanxin, Y. Na, and A Yong, "Preparation of uniform highly dispersed Mg–Al-LDHs and their adsorption performance for chloride ions," *Industrial & Engineering Chemistry Research*, vol. 59, no. 22, pp. 10697–10704, 2020.

[15] X. H. Wang, J. X. Xu, and Q. P. Tan, "Effect of nitrite intercalated Mg-Al layered double hydroxides on mortar durability under $Cl^-$ and $SO^{2-}_4$ coexisting environment," *Journal of Central South University*, vol. 29, no. 2, pp. 546–560, 2022.

[16] Y. Xu, W. Wang, L. Liang, and S. Zhang, "Chloride ions adsorption behavior on CaMnFe-LDHs and solidification performance of chloride ions on cement slurry blocks containing CaMnFe-LDHs," *Desalination and Water Treatment*, vol. 260, pp. 139–147, 2022.

[17] H. Hayatdavoudi and M. Rahsepar, "Smart inhibition action of layered double hydroxide nanocontainers in zinc-rich epoxy coating for active corrosion protection of carbon steel substrate," *Journal of Alloys and Compounds*, vol. 711, pp. 560–567, 2017.

[18] J. X. Xu, J. F. Wei, G. X. Ma, and Q. Tan, "Effect of MgAl-$NO_2$ LDHs inhibitor on steel corrosion in chloride-free and contaminated simulated carbonated concrete pore solutions," *Corrosion Science*, vol. 176, Article ID 108940, 2020.

[19] S. Yoon, J. Moon, S. Bae, X. Duan, E. P. Giannelis, and P. M. Monteiro, "Chloride adsorption by calcined layered double hydroxides inhardened Portland cement paste," *Materials Chemistry and Physics & Physics*, vol. 145, no. 3, pp. 376–386, 2014.

[20] L. Yang, M. Chen, Z. Lu et al., "Synthesis of CaFeAl layered double hydroxides 2D nanosheets and the adsorption behaviour of chloride in simulated marine concrete," *Cement and Concrete Composites*, vol. 114, Article ID 103817, 2020.

[21] J. Xu, Y. Song, Q. Tan, and L. Jiang, "Chloride absorption by nitrate, nitrite and aminobenzoate intercalated layered double hydroxides," *Journal of Materials Science*, vol. 52, no. 10, pp. 5908–5916, 2017.

[22] D. D. Wang, Q. Zhu, Y. Y. Su, J. Li, A. Wang, and Z. Xing, "Preparation of MgAlFe-LDHs as a deicer corrosion inhibitor to reduce corrosion of chloride ions in deicing salts," *Ecotoxicology and Environmental Safety*, vol. 174, pp. 164–174, 2019.

[23] Y. B. Song, J. X. Xu, and L. H. Jiang, "Anti-corrosion performance of $NO_3^-/NO_2^-$ intercalation of MgAl-LDHs in simulated concrete pore solution," *Journal of Zhejiang University (Engineering Science)*, vol. 52, pp. 2397–2405, 2018.

[24] L. Guo, Y. Y. Wu, P. Duan, and Z Zhang, "Improving sulfate attack resistance of concrete by using calcined Mg-Al-CO3 LDHs: adsorption behavior and mechanism," *Construction and Building Materials*, vol. 232, Article ID 117256, 2020.

[25] Z. G. Li, W. J. Ji, and Y. Li, "Research progress on application of layered double hydroxides in cement concrete," *Concrete*, vol. 1, pp. 25–30, 2021.